Available online at www.sciencedirect.com

ScienceDirect

Procedia Structural Integrity 24 (2019) 738–745

Structural Integrity Procedia

www.elsevier.com/locate/procedia

AIAS 2019 International Conference on Stress Analysis

Fracture locus of a CORTEN steel: Finite Element calibration based on experimental results

L. Maccioni[a], F. Concli[a,] *

[a]*Free University of Bolzano/Bozen, Faculty of Science and Technology, Piazza università 5, Bolzano 39100, Italy*

Abstract

In order to protect low-alloy steel from corrosion in outdoor applications, it is common practice to use surface treatments e.g. painting or galvanization. The costs of these specific treatments and further maintenance can be reduced by exploiting weathering steel, the so-called CORTEN steel. The rust of this material forms a protective layer, adherent and self-regenerative, capable to stop the oxidation of the raw material. This characteristic, called self-passivation, is achieved by adding Cu, Cr and P in the alloy. Furthermore, its natural rust-color inspired architects, artists and civil engineers that start using CORTEN for bridges, building facades, artworks etc.. The harmony of CORTEN with natural environments boosts its application for guardrails (safety barriers) along the highway and alpine roads of the South-Tyrolean region.
These components, in addition to aesthetic characteristics, have to fulfill safety requirements, especially during crash events.
During an impact, the main goal of guardrails is to absorb and dissipate energy. Large deformations take place. Therefore, the most important mechanical characteristic for guardrails' materials is the tenacity related to the ductile behavior. However, despite CORTEN guardrails are homologated through experimental tests, in some specific conditions the passivation process could fail. Therefore, its energy absorption capabilities can be jeopardized by corrosion. In order to verify and/or optimize specific guardrails' geometries for safety applications, it is important to be able to model the ductile behavior and fracture locus of CORTEN within finite elements.
The goal of this paper is to characterize the ductile behavior of CORTEN through experimental quasi-static tests with different geometries, thus different level of triaxiality. The test configurations were numerically reproduced, to retrieve the actual stress state, quantify the plastic strain at failure and calibrate a ductile damage model.

Keywords: ductile damage, fracture locus, experiments, FEM, CORTEN, DIC

* Corresponding author. Tel.: +39 0471 017748; fax: +39 0471 017009.
E-mail address: franco.concli@unibz.it

10.1016/j.prostr.2020.02.065

1. Introduction

A new weathering steel was launched by the "U.S. Steels" in the early Thirties (Decker et al., 2008). In order to underline its resistance to CORrosion and its TENsile strength, the self-passivating low-alloy steel was called CORTEN, but other nomenclatures are also used e.g. COR-TEN, Corten, Cor-Ten. Its composition underwent some adjustments in the years (Revie, 2011) and nowadays, in Europe, weathering steels are outlined in the DIN EN 10020. Its strength characteristics, comparable to those of other construction steels (Yield strength typically among 235-355 MPa), were not the main drivers for its exploitation in industry and interest in research. Indeed, CORTEN was initially exploited in the railway sector (Dunkley, 1967) in order to decrease the weathering of carriages. It was also used in bridges (Fischer, 1995) with the aim of overcoming the need of painting and maintenance. For aesthetical reasons, its application was extended to facade of buildings (Mostafavi and Leatherbarrow, 1993) and it was used also for many outdoor artworks e.g. (Web Reference 1).

Researchers studied the CORTEN corrosion behavior in different environments (Kamimura et al., 2006; Mocillo et al., 2013). Indeed, CORTEN requires wet/dry cycles to succeed in creating a protective layer of rust (Schmitt and Gallagher, 1969). In addition, close to the marine environment, this phenomenon is negatively affected by the presence of Cl^- (Zhang et al., 2013). In polluting environment, the passivation process, especially with high humidity, is prevented by SO_2 (Wang et al., 1997). Moreover, the corrosion behavior was studied varying alloy elements (Wang et al., 2014), metal microstructures (Guo et al., 2009) and surfaces finishes (Chiavari et al., 2012).

Nowadays, guardrails of the Brenner Highway (Web Reference 2) and many local roads of the alpine region South-Tyrol are in CORTEN. This is because the natural color of CORTEN (brown) presents a good visual impact in this UNESCO world heritage. Secondly, the low (expected) maintenance costs favored its exploitation.

Despite homologation tests are mandatory in this field (Web Reference 3), in some specific areas the CORTEN guardrails are not exempt from corrosion (Deflorian and Rossi, 2002). Therefore, it is possible that the resistance and energy absorption capabilities of the structures are compromised by lacking passivation and the consequent corrosion.

In order to assert the safety performances of CORTEN guardrails by means of FE (finite element) crash simulations, it is essential to characterize the constitutive law (Whitworth et al., 2004) and fine-tune the fracture locus of the material (Ren and Vesenjak, 2005). Eventually, such FE models could be useful for the reconstruction of crash events.

A first work aimed to characterize the ductile behavior of the CORTEN through experimental quasi-static tests with different geometries, thus different level of triaxialities, was presented by the authors (Concli and Maccioni, 2019). However, the tested CORTEN samples had a thickness of 8 mm. This paper aims to repeat the experiments with similar samples, having a different thickness (2 mm) to possibly highlight the effects of the rolling process on the ductile behavior of CORTEN. In addition, the tests were numerically reproduced, to retrieve the actual stress state, quantify the plastic strain at failure and calibrate a ductile damage model with additional tests.

2. Materials and Methods

In this study, two series of samples made of CORTEN (S355J0WP) were used. Different geometries were laser cut from 8 mm and 2 mm thick sheets (Fig. 1).

Dedicated mono-axial tests were performed on a MTS Criterion 45 testing machine that is capable to apply loads up to 100kN. Applied force and crosshead displacement were acquired for each sample. For smooth samples, also the deformation, measured through an extensometer, was acquired.

The constitutive law in the plastic (hardening) region can be described through Equation 1, also called Voce law (Voce, 1948; Voce, 1955), where each constant can be found through an inverse numerical procedure.

$$\sigma = C_1 + C_2\left(1 - e^{-C_3\varepsilon_p}\right) + C_4\varepsilon_p \tag{1}$$

The constants C_i are the yielding stress, the linear coefficient, the exponential coefficient and the so-called exponential saturation parameter respectively and ε_p is the accumulated plastic strain.

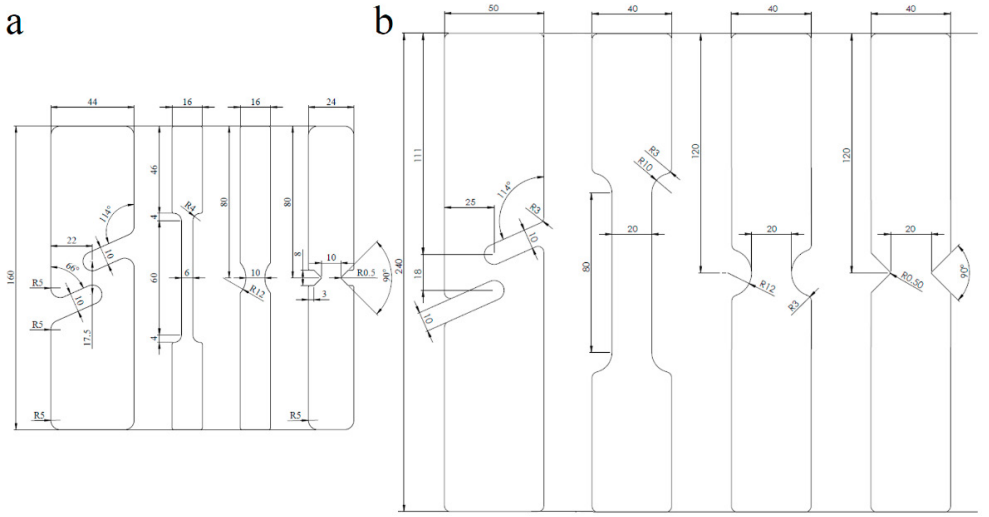

Fig. 1. Geometries of the samples (a) 8 mm of thickness (b) 2 mm of thickness - from left: #1.1, #2.1, #3.1, #4.1, #1.2, #2.2, #3.2, #4.2 (the first number represents the series – 1 for 8 mm thickness, 2 for 2 mm thickness; the second number represent the geometry – 1 for shear samples, 2 for smooth samples, 3 for round-notched samples, 4 for V-notched samples)

For each sample geometry, a simulation has been performed. The F-s (Force – crosshead displacement) curve (Fig. 2) obtained numerically was compared with the experimental (measured) one. Through this iterative process, it was possible to calibrate the constitutive law also beyond the necking. Table 1 reports the results of the calibration.

Table 1. Parameters of the Voce law for the CORTEN steel

C_1 [MPa]	C_2 [MPa]	C_3 [-]	C_4 [MPa]
390	250	11	200

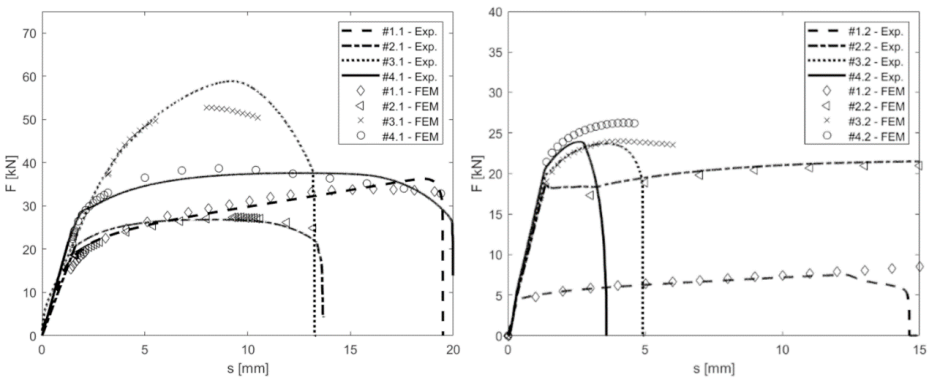

Fig. 2. Force-displacement diagrams - numerical vs. experimental; Left: geometries #X.1; Right: geometries #X.2

In the years, many scholars presented ductile damage models. Rice and Tracey (1969) were pioneers in this regard and proposed a model that recognizes stress triaxiality as fundamental factor in the failure of metals (exponential decreasing function). Additional models were developed by Hancock and Mackenzie (1976) in which the effects of temperature and strain-rate were included. Further improvements were proposed by Johnson and Cook (1983) and Mirza et al. (1997). In all these models, the stress triaxiality η, defined as in Equation 2, is a function of the plastic strain at fracture ε_{peeq}.

$$\eta = \frac{\sum \frac{\sigma_i}{3}}{\sqrt{\frac{1}{2}\left[\sum\left(\sigma_i - \sigma_j\right)^2\right]}} \tag{2}$$

However, studies performed by Bao (2003), Bao and Wierzbicki (2004), Bao (2005) and Gilioli et al., (2015) have demonstrated that the influence of triaxiality cannot be modelled through a monotonic function. Suárez et al. (2018) shown that the fracture locus presents three main triaxiality regions involving different failure mechanisms (Fig. 3). For low values of triaxiality, shearing is the main mechanism of failure; for high values of triaxiality, the nucleation-growth-coalescence is the main mechanism of fracture. A combination of these two mechanisms can be found for intermediate values of triaxiality that is the region explored in the present work. Further tests are planned in order to study the $\eta - \varepsilon_{peeq}$ relationship also for different values of triaxiality. The influence of strain rate and temperature variation were not included in this paper.

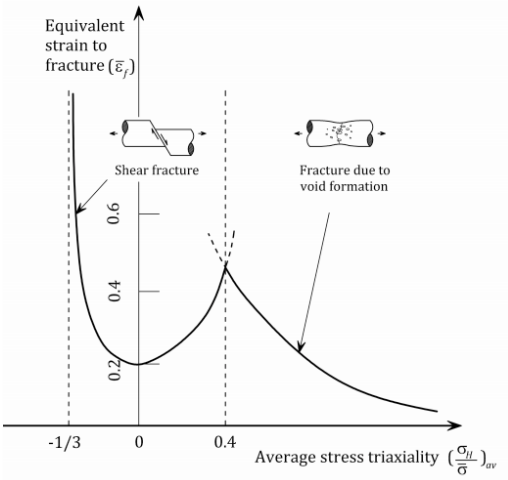

Fig. 3. Relationship between the average stress triaxiality and the equivalent strain to fracture by Suárez et al. (2018)

Fig. 2 shows the samples' geometries exploited for the calibration of the fracture locus. Each sample was brought up to rupture during the tensile test. By means of the open-source free software Code-Aster, the tests were reproduced numerically as described in (Concli and Gilioli, 2019; Concli et al., 2019).

The authors exploited an open-source software since the absence of licenses allows highly parallelized computations. Simulations were performed up to the displacement that experimentally (crosshead) corresponds to the failure (Fig.s 4 and 5). ε_{peeq} (equivalent plastic strain at fracture) and η (triaxiality in the position that experimentally

cracks) were obtained from the numerical simulations (Fig. 6). The values are reported in Table 2. After a root mean square interpolation, the equation describing the fracture locus results in Equation 3.

$$\varepsilon_{peeq} = 39.318 \cdot \eta^2 - 21.32 \cdot \eta + 3.3833 \tag{3}$$

Table 2. triaxiality η and equivalent plastic strain at fracture ε_{peeq}

	Sample geometry							
	#1.1	#2.1	#3.1	#4.1	#1.2	#2.2	#3.2	#4.2
η	0.25	0.23	0.21	0.39	-0.30	0.27	0.55	0.36
ε_{peeq}	1.35	0.47	0.75	1.22	0.81	0.57	0.11	0.57

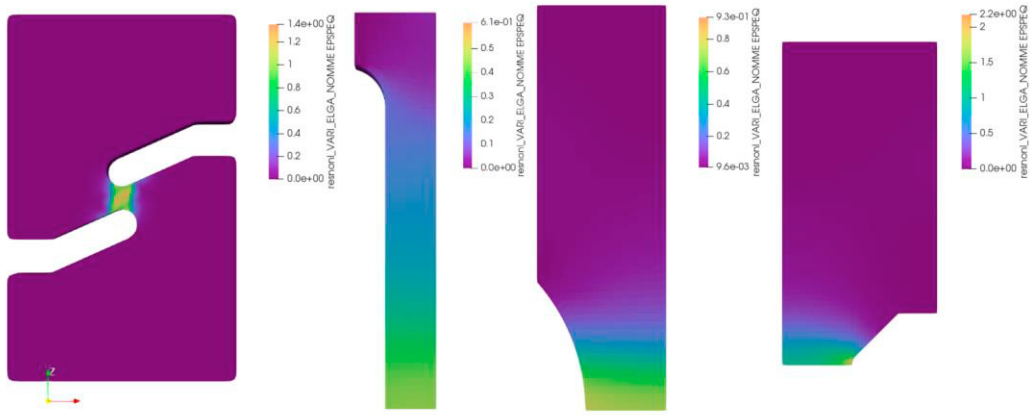

Fig. 4. ε_{peeq}, samples #1.1, #2.1, #3.1 and #4.1

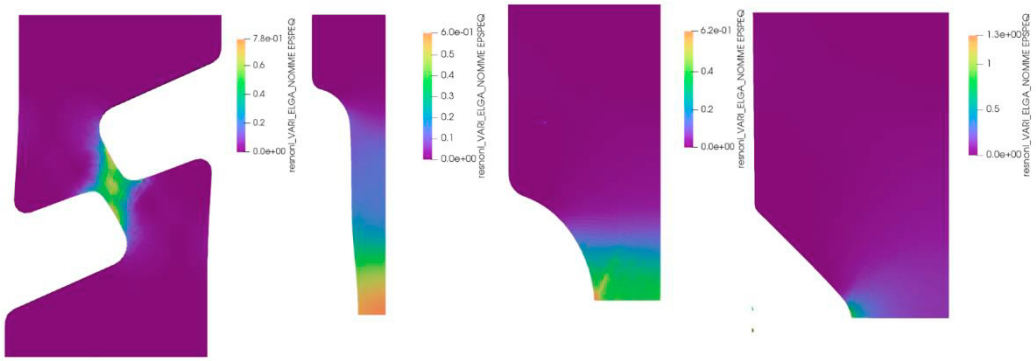

Fig. 5. ε_{peeq}, samples #1.2, #221, #3.2 and #4.2

Fig. 6 shows the 7 points ($\eta - \varepsilon_{peeq}$) falling in the med-range triaxiality interval (interpolated through Equation 3). It is possible to notice that the scatter of the points (except for the shear sample that falls out of the range #1.2, $\eta = -0.3$) fits the quadratic Johnson & Cook curve.

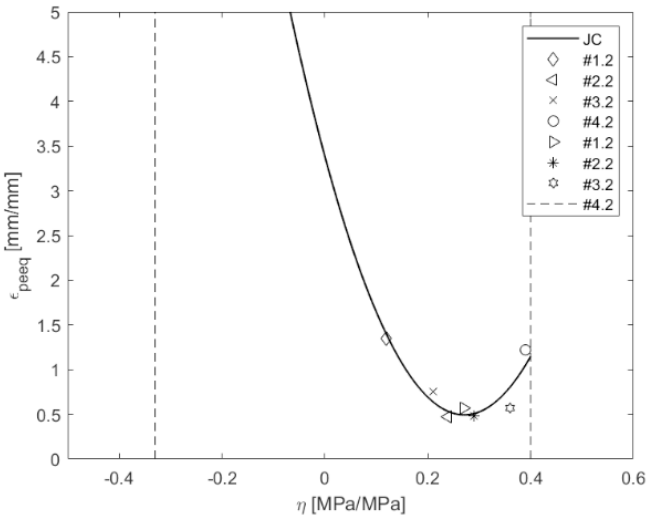

Fig. 6. Fracture Locus

For completeness, with DIC (Digital Image Correlation) measurements were also performed during the tests. DIC is an optical method capable to measure full-field displacement and strains. Before the tests, each sample is painted with a surface texture. Picture of the sample were acquired during the experimental tests by means of a reflex camera having 32 MPixel. A mapping function can be derived from a comparison of a set of sub-image pairs over the whole images, i.e. at different time steps. In particular, images were captured every 3 s (e.g. every 0.05 mm of displacement of the crosshead). The coordinates x_i, y_j (of the undeformed sample) and x_i^*, y_j^* (at a certain time step) are related by the translations that occur between the subsequent images. This allows the reconstruction of the displacement- and successively the strain-field. The cross-correlation was made with a facet size of 100 pixels and a point distance of 100 pixels.

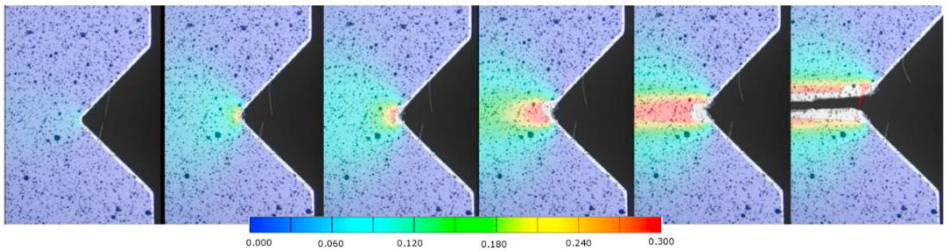

Fig. 7. DIC measurements – strain field

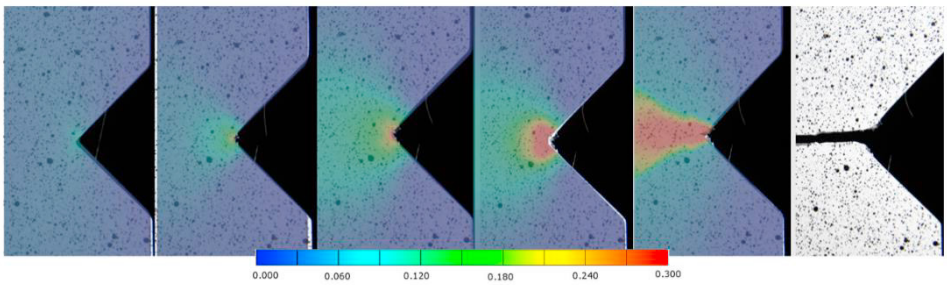

Fig. 8. FEM results – strain field

Fig. 7 shows the deformations of the sample #4.2 elaborated with DIC. On the right-hand side, it can be appreciated how, after the failure, large residual plastic deformations remain in the material. Fig. 8 reports the deformations calculated numerically overlapping real pictures of the sample. The contours are comparable just for the first three images, i.e. before the cracking of the material (not considered by the FE model). Indeed, while in the real sample a crack nucleates and propagates changing the topology of the sample, in the FEM model the upper and the lower part of the sample remain connected; consequently, the strain fields result different. To this respect, a FE model with the possibility to detach the mesh elements once ε_{peeq} locally overcome the limit (Fig. 6), ensure a more realistic strain field (Concli and Gilioli, 2018).

3. Conclusions

In this study, the ductile fracture model proposed by Johnson and Cook (1983) has been calibrated for a CORTEN steel (S355J0WP). Through an iterative procedure, the constitutive law was found. Afterward, the fracture locus was fine-tuned based on seven samples differing in thickness and geometry. An open-source FEM software Code_Aster was used. In addition, DIC was tested and will be systematically used in the following analysis.

The effect of temperature and strain rate were neglected but will be included in future studies aimed to extend the fracture locus of CORTEN also for the low- and high-triaxiality regions. In addition, some preliminary tests have shown a slight anisotropy in the CORTEN (2 mm thick sheet metal) depending on the rolling direction. Therefore, further studies will be conducted on low thickness samples, cut from the same sheet, considering different rolling directions. Eventually, the tests were conducted on samples not yet passivated; a further step forward will be the repetition of the experiments with passivated ones.
Furthermore, the model will be used for the study of the behaviour of a guardrail in CORTEN during an impact.

4. Acknowledgment

The authors would like to thank A.ERRE Srl di Serravalle Pistoiese (PT) Italy http://www.aerrecarpenteria.it/ for the financial support.

References

Bao, Y. 2003. Prediction of ductile crack formation in uncracked bodies (Doctoral dissertation, Massachusetts Institute of Technology).

Bao, Y. 2005. Dependence of ductile crack formation in tensile tests on stress triaxiality, stress and strain ratios. Engineering fracture mechanics, 72(4), 505-522.

Bao, Y., Wierzbicki, T. 2004. On fracture locus in the equivalent strain and stress triaxiality space. International Journal of Mechanical Sciences, 46(1), 81-98.

Chiavari, C., Bernardi, E., Martini, C., Passarini, F., Motori, A., Bignozzi, M. C., 2012. Atmospheric corrosion of Cor-Ten steel with different surface finish: Accelerated ageing and metal release. Materials Chemistry and Physics, 136(2-3), 477-486.

Concli, F., Maccioni, L., 2019. Experimental-numerical calibration of the fracture locus of a weathering steel. In: 9th International Conference on Computational Methods and Experiments in Material and Contact Characterization, 22–24 May, Lisbon (Portugal).

Concli, F., Gilioli, A. 2019. Numerical and experimental assessment of the mechanical properties of 3D printed 18-Ni300 steel trabecular structures produced by Selective Laser Melting–a lean design approach. Virtual and Physical Prototyping, 14(3), 267-276.

Concli, F., Gilioli, A., Nalli, F. 2019. Experimental–numerical assessment of ductile failure of Additive Manufacturing selective laser melting reticular structures made of Al A357. Proceedings of the Institution of Mechanical Engineers, Part C: Journal of Mechanical Engineering Science, 0954406219832333.

Concli, F., Gilioli, A., 2018. Numerical and experimental assessment of the static behavior of 3d printed reticular Al structures produced by Selective Laser Melting: progressive damage and failure. Procedia Structural Integrity,12, 204-212.

Decker, P., Brüggerhoff, S., Eggert, G., 2008. To coat or not to coat? The maintenance of Cor-Ten® sculptures, Material and corrosion, 59(3), 239–247.

Deflorian, F., Rossi, S., 2002. Premature corrosion failure of structural highway components made from weathering steel. Engineering Failure Analysis, 9(5), 541-551.

Dunkley, F. G., 1967. Painting of railway rolling stock, Journal of the Institution of Locomotive Engineers, 57(319), 509–553.

Fischer, M., 1995. Weathering Steel in Bridges. Structural Engineering International, 5(1), 51–54.

Gilioli, A., Manes, A., Giglio, M., Wierzbicki, T. 2015. Predicting ballistic impact failure of aluminum 6061-T6 with the rate-independent Bao–Wierzbicki fracture model. International Journal of impact engineering, 76, 207-220.

Guo, J., Yang, S., Shang, C., Wang, Y., He, X., 2009. Influence of carbon content and microstructure on corrosion behavior of low alloy steels in a Cl− containing environment. Corrosion Science, 51(2), 242-251.

Hancock, J. W., Mackenzie, A. C. 1976. On the mechanisms of ductile failure in high-strength steels subjected to multi-axial stress-states. Journal of the Mechanics and Physics of Solids, 24(2-3), 147-160.

Johnson, G.R., Cook, W.H. 1983. A Constitutive Model and Data for Metals Subjected to Large Strains, High Strain Rates, and High Temperatures. Proceedings 7th International Symposium on Ballistics, The Hague, 541-547.

Kamimura, T., Hara, S., Miyuki, H., Yamashita, M., Uchida, H., 2006. Composition and protective ability of rust layer formed on weathering steel exposed to various environments," Corrosion Science, 48(9), 2799–2812.

Mirza, M. S., Barton, D. C., Church, P., Sturges, J. L. 1997. Ductile fracture of pure copper: An experimental and numerical study. Le Journal de Physique IV, 7(C3), C3-891.

Morcillo, M., Chico, B., Díaz, I., Cano, H., de la Fuente, D., 2013. Atmospheric corrosion data of weathering steels. A review. Corrosion. Science, 77, 6–24.

Mostafavi, D., Leatherbarrow, M., 1993. On weathering: the life of buildings in time. MIT Press.

Ren, Z., Vesenjak, M., 2005. Computational and experimental crash analysis of the road safety barrier. Engineering Failure Analysis, 12(6), 963-973.

Revie, R. W., 2011. Uhlig's Corrosion Handbook: Third Edition.

Rice, J. R., Tracey, D. M. 1969. On the ductile enlargement of voids in triaxial stress fields. Journal of the Mechanics and Physics of Solids, 17(3), 201-217.

Schmitt, R. J., Gallagher, W. P., 1969. Unpainted high strength low alloy steel. Materials Protection. 8(12), 71-77.

Suárez, F., Gálvez, J., Cendón, D., Atienza, J. 2018. Distinct Fracture Patterns in Construction Steels for Reinforced Concrete under Quasistatic Loading—A Review. Metals, 8(3), 171.

Voce, E., 1948. The relationship between stress and strain for homogeneous deformation. Journal of the Institute of Metals, 74, 537–562.

Voce, E., 1955. A practical strain-hardening function. Metallurgia, 55, 219–226.

Wang, J. H., Wei, F. I., Chang, Y. S., Shih, H. C., 1997. The corrosion mechanisms of carbon steel and weathering steel in SO2 polluted atmospheres. Materials Chemistry and Physics, 47(1), 1-8.

Wang, R., Luo, S., Liu, M., Xue, Y., 2014. Electrochemical corrosion performance of Cr and Al alloy steels using a J55 carbon steel as base alloy. Corrosion Science, 85, 270-279.

Web reference 1: "https://www.pinterest.it/trackdesign9867/corten+art/?lp=true.".

Web Reference 2: "https://www.autobrennero.it/it/la-rete-autostradale/la-sicurezza/barriere-sicurezza/."

Web Reference 3: "https://www.autobrennero.it/documenti/4_Area_tecnica/Pubblicazioni/2010/barriere_sicurezza_A22.pdf"

Whitworth, H. A., Bendidi, R., Marzougui, D., Reiss, R., 2004. Finite element modeling of the crash performance of roadside barriers. International journal of crashworthiness, 9(1), 35-43.

Zhang, Q. C., Wu, J. S., Wang, J. J., Zheng, W. L., Chen, J. G., Li, A. B., 2003. Corrosion behavior of weathering steel in marine atmosphere. Materials Chemistry and Physics, 77(2), 603–608.